Gold-based carbon-supported bimetallic catalysts for energy storage and biomedical applications

C.I. Oseghale[1a, c]*, A. H. Abdalla[d], M. K. H. Uddin[b] and P. J. Hall[a]

[a]Department of Chemical & Biological Engineering, University of Sheffield, Mappin Street, Sheffield, S1 3JD, England, UK

[b]Department of Material Sciences and Engineering, Kroto Research Institute. University of Sheffield, Broad Lane Street, Sheffield, S3 7HQ, England, UK

[c]Department of Chemical Engineering, University of Port Harcourt, East-West Road, Choba, Port Harcourt, Rivers State, Nigeria.

[d]Department of Chemistry, Faculty of Arts and Science-Traghen, University Of Sebha, Libya

Abstract

In this study, the controlled synthesis of highly reactive gold palladium bimetallic nanostructured catalyst, using polyvinyl pyrrolidone stabiliser, has been proposed. In order to determine the morphology, biocompatibility and to explore the chemistry of the produced $Au_{0.8}Pd_{0.2}$-C samples, microscopic examinations, cell viability and Raman spectroscopy technique were performed. The XRD pattern displayed a well-defined fcc crystalline structure for the $Au_{0.8}Pd_{0.2}$-C and Pd-C catalysts. The presence of Au in $Au_{0.8}Pd_{0.2}$-C electrodes promotes a positive effect, which was confirmed by the appearance of a broad peak in the region of H_2 adsorption/desorption, suggesting that the H_2 adsorption/desorption processes on the surface of catalyst were favored. Standard MTT assay performed on the $Au_{0.8}Pd_{0.2}$-C samples displayed a decreased cellular response with respect to the control group; however, cell confluency throughout the tissue culture plate suggested biocompatibility of the given sample. Moreover, when the $Au_{0.8}Pd_{0.2}$-C catalyst was chemically tested by Raman spectroscopy, the presence of Au and Pd ions was confirmed.

Keywords: Chemical synthesis, Bimetallic Nanostructure, Biomaterials, Low-cost, Batteries

1 Introduction

The growing demand for energy has seen an increase in the research and development of new energy technologies from renewable sources [1-3]. Electrochemical energy storage

1* Corresponding authors. Chemical and Biological Engineering, University of Sheffield, Sir Robert Hadfield Building, Mappin Street, Sheffield S1 3JD, England, UK. Tel: +44(0)1142227555. Fax: +44(0)1142227501. E-mail: oselu4jesu@gmail.com

technologies such as batteries require effective electrocatalytic materials to upgrade and improve performance. The preparation of high performance heterogeneous bimetallic catalysts will enhance the widespread utilisation of aqueous battery technology [4]. Gold and gold-based catalysts are very effective for both heterogeneous and homogenous catalysis. In particular, the excellent performance of gold-based catalysts is widely recognized, after the pioneering work of Haruta and co-workers, in the redox reaction of the low-temperature carbon monoxide oxidation reaction [5-10]. Progress will strongly depend on new effective catalysts for high energy storage applications. The environmental challenges posed by the use of such highly toxic materials (Pd, Ni, and Cd) in electrodes need to be avoided by developing poisoning-resistant and environmentally friendly materials.

The key to effective utilisation of intermit renewable energy is the development of large-scale energy storage. Rechargeable batteries play a prominent role in this context. In particular, aqueous electrolyte rechargeable batteries, based on alkali ions, are promising candidates because of their inherent safety, low cost, longevity, and tolerance to over-charge or discharge [11, 12]. Potassium hydroxide has very good current-conducting and low internal resistance properties. Potassium is more naturally abundant element than sodium and lithium metals, which suffer low capacity issues and poor stability [4, 13].

The unique properties of gold at the nanoscale – for instance: low electrical resistivity, inertness and resistance to sulfur-based tarnishing – also render it suitable for implantation due to its biocompatibility, when compared with most other metals [14, 15]. Recent advances in synthesis techniques and biomolecular engineered gold nanoparticles have led to medical applications in the areas of biosensors, gene and photothermal therapy, targeted drug delivery, tissue engineering, and disease therapy [16-19].

In this article, we present a gold-palladium catalyst on a carbon black support for both energy storage and biocompatible applications. Following the previous synthesis route by Oseghale et al. 2016 [20], a two-stage preparation method of AuPd on carbon black was carried out at room temperature. The palladium precursor was stabilised in solution with polyvinylpyrrolodone (PVP) using excess sodium borohydride solution as a reducing agent. The physical, electrochemical and biocompatibility measurements were performed, to determine the performance characteristics of the as-prepared catalysts.

2 Experiment and methods

2.1 Synthesis of $Au_{0.8}Pd_{0.2}$-C catalysts

The $Au_{0.8}Pd_{0.2}$-C catalysts were prepared by measuring 140 mg of polyvinylpyrrolidone (PVP, 1.30 mmol of monomeric units, mol.wt. = 40,000, 99.9% Sigma-Aldrich), 10 mL of fresh deionized water (18.2 M∧.cm^{-1}, Purelab option ELGA) and 0.42 mL of 0.062 mol/L palladium chloride ($PdCl_2$, 99.9% Sigma-Aldrich)). The obtained solution was purged with argon gas for approximately 1h in order to remove the dissolved oxygen. Then, 10 mL of freshly prepared 1M sodium borohydride ($NaBH_4$, 99%, Aldrich) was added dropwise to the $PdCl_2$-PVP solution, with continuous stirring, and was protected with argon gas. The reaction was allowed to proceed for 1h to yield PVP-stabilised Pd nanoparticles in solution. 6.3 mL of freshly prepared, deaerated $HAuCl_4.3H_2O$ solution (0.05 mol/L, 99.9% Sigma-Aldrich) was added quickly to the Pd-PVP nanoparticles in solution and stirred for 1h under argon protection. As the redox potential of Au^{3+}/Au (1.498V) is higher than that of Pd^{2+}/Pd (0.987V), Au (III) is reduced to Au and therefore Pd (core)-Au (shell) particles were formed (see Figure 1).

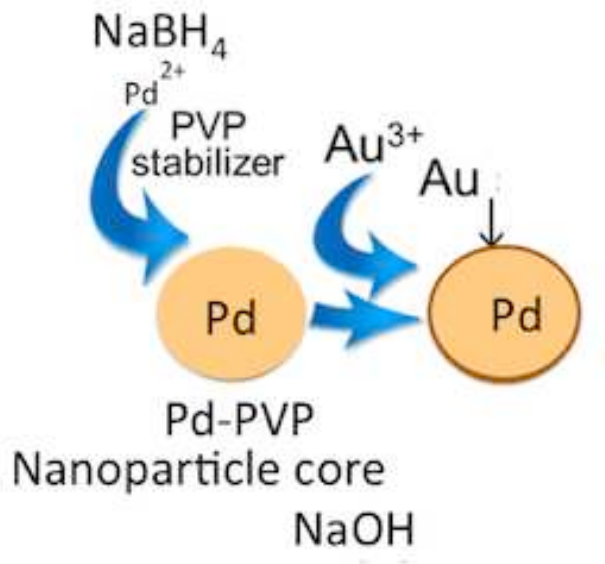

Figure 1*: Diagram illustrating the use of PVP stabilised chemical reduction synthesis for the preparation of $Au_{0.8}Pd_{0.2}$-C_{PVP} catalyst[20]*

Within a few minutes of sol generation, the sol was immobilised by adding Vulcan XC72 (Cabot) under vigorous stirring for 30 min and was then allowed to settle for 30 min. The resulting carbon black-supported $Au_{0.8}Pd_{0.2}$ catalysts were obtained by filtering the resultant

solution using Whatman cellulose nitrate filter paper. The $Au_{0.8}Pd_{0.2}$-C catalysts were washed several times with deionized water, to remove any free PVP macromolecules not bound to $Au_{0.8}Pd_{0.2}$-C catalysts, and until no chloride ion (Cl^-) was detected in the filtrate solution. The $Au_{0.8}Pd_{0.2}$-C catalysts were dried under vacuum at 80 ^oC overnight to obtain the final catalysts. Using this synthesis procedure, 20 wt.% AuPd-C catalysts with Au:Pd ratio of 80:20 were prepared. The $Au_{0.8}Pd_{0.2}$-C catalysts were denoted as Au_xPd_y (x, y stand for the atomic ration of each element) based on the ICP-OES results.

2.2 Physiochemical Characterization of Catalysts

The compositional analysis was determined using a Spectro-Ciros-Vision ICP-OES for the metal loading in the samples and shown to be consistent with the calculated from preparation procedure. X-ray diffraction (XRD) patterns of the sample were obtained using an X-ray diffractometer (model D2 Phaser Bruker Ltd) with CuKα1 radiation (λ = 1.5406 Armstrong) and a graphite monochromator, maintained at a tube voltage and current of 30 kV, 10 mA. The 2θ angular region between 15^o – 90^o were explored at a scan rate (1^o min^{-1}), with a step size of 0.1 and increment (i.e. step size between data point) of 0.02. The primary divergence slit of 0.6 mm was used and the Ni K-beta filter was not fitted because of the carbon black support. Scanning electron microscopy (SEM) was used to obtain micrographs, along with Phillips Inspect F.USA, with beam energy of 15kV. For further chemical analysis, energy dispersive x–ray (EDS) was used with EDAX Genesis software. All samples were prepared by dispersing 1 mg of Pd-C catalysts in 1 mL of 96% ethanol and sonicated for 1 minute in a water bath. 10 μL of the paste was cast on Joel 10 mm x 10 mm diameter plain stubs and dried at room temperature. Raman spectroscopy was used to obtain spectra of the gold and palladium samples, using a Thermo scientific™ DXR™ Raman microscope under shifted spectrum (cm^{-1}) format, between the range of 400 – 4000 cm^{-1}. The individual spectrum was obtained using 532 nm lasers and the data analysis of the obtained spectra was carried out using OMNIC® software.

2.3 Working Electrode Preparation

The working electrode was polished to a mirror finish using 0.5 and 0.05 μm alumina suspensions sequentially before use. An appropriate dilution ratio of catalysts, analytical

grade ethanol (96%, Aldrich) and 5wt.% Nafion solution (99.99%, Aldrich) were mixed for 1h. On the surface of the glassy carbon electrode (GCE) (OD: 6 mm ID: 3.0 mm), 9μL slurry was spread and dried overnight at 80 ^{o}C to obtain the working electrodes. The apparent surface area of the GCE was 0.07 cm^2. The 20wt.% $Au_{0.8}Pd_{0.2}$-C and Pd-C loading of the electrode was 7 g/m^2.

2.4 Cyclic Voltammetry (CV) Experiment

All electrochemical experiments were carried out at room temperature, using a conventional three-electrode cell configuration, with a Solartron Analytical Instrument, model 1400/1470E. The working electrode was a modified inert GCE (internal diameter: 3.0 mm), a Pt wire (0.5 mm diameter) was the counter electrode and an $Ag/AgCl_{sat.KCl}$, standard electrode (0.256V/NHE or 0.197V/SHE) was used as the reference electrode. CV experiments were performed in 1 M KOH, in the potential range -1 V to +0.4 V versus reference electrode ($Ag/AgCl$, KCl_{std}), at a scan rate of 50 mVs^{-1}, to establish a correlation between electrochemical behaviour and catalytic performance in the oxidation of potassium hydroxide. All experimental data were analysed using the MultiStat Data software for evaluations and calculations.

Chronoamperometry (CA) is an electroanalytical technique typically used to investigate the catalyst stability, kinetics, mechanism and the determination of diffusion coefficients of the electrochemical system. It involves potential voltage excitation of -0.3 V for 1000 seconds and gives a resulting current density. This method requires semi-infinite linear diffusion (i.e. an unstirred solution, linear diffusion to the electrode surface, a planar electrode and a supporting electrolyte to insure the absence of ion migration) and no other reactions.

2.5 In vitro cell viability analysis

Biocompatibility of the $Au_{0.8}Pd_{0.2}$-C sample produced was evaluated using cultured human oral fibroblasts (Passage 4) and the cellular response was analyzed using the standard 3-(4,5-Dimethylthiazol-2-YI)-2,5-Diphenyltetrazolium Bromide (MTT) assay protocol [21]. The prepared specimen was sterilised in an autoclave (15 min at 121°C/ 15 psi). The cells were cultured in DMEM media, supplemented with 10% FCS, 1% glutamine and 1% penicillin/streptomycin (Sigma-Aldrich UK). Then, cells were allowed to confluent (100%)

over the surface of the tissue culture plate and were detached using EDTA trypsin (Sigma-Aldrich, UK). A 24-well plate was used for cell seeding, containing the test and control samples with a seeding density of 1.25×10^4 cells/ml. A non-material and material control (negative) and (positive) were introduced for the direct correlation. Material and cells were both incubated at 37°C in a 5% CO_2 atmosphere for 24 h [21].

For the quantitative measurement, an MTT assay was carried out individually on the respective prepared specimen. A MTT solution of 0.1ml was added aseptically to each well and left for incubation at 37 °C for 4 hrs. Similarly, cells were then lysed with isopropanol and the intensity of the colored solution was measured using a photo spectrometer at a wavelength of 570 nm [21, 22].

3 Results and discussion

3.1 Crystallography of $Au_{0.8}Pd_{0.2}$-C and Pd-C catalysts

The crystal phases of the $Au_{0.8}Pd_{0.2}$-C catalysts were characterised using XRD. The diffraction peaks are given in Figure 2. The diffraction patterns presented five peaks for $Au_{0.8}Pd_{0.2}$-C (at 2theta: 38.29^o, 44.58^o, 64.75^o, 77.84^o, and 82.11^o) and four peaks for the Pd-C catalysts (40.06^o, 45.76^o, 67.89^o, and 80.16^o) corresponding to the (111), (200), (220), (311), and (222) planes [23]. These peaks confirm Au is present in the face-centered cubic (fcc) lattice structure in the $Au_{0.8}Pd_{0.2}$-C catalysts [24, 25]. It is observed that the higher *d* space for $Au_{0.8}Pd_{0.2}$-C (d_{111} = 2.3234 Å) could be due to the lower (111) peak of Au (d_{111} = 2.3503 Å) because of the incorporation of Pd atoms, indicating the bimetallic structure is on the carbon support [24, 26]. The 2theta values of the reflection peaks of the $Au_{0.8}Pd_{0.2}$-C catalyst (Figure 2a) show a shift to lower angles for all peaks related to Pd-C catalysts (Figure 2b). This indicates that the Pd atoms in the $Au_{0.8}Pd_{0.2}$-C catalysts did not disperse into the Au lattice, forming an alloy structure [25, 27, 28] or a simple aggregate of metal nanoparticles [28]. This is in agreement with the analysis of the extent of alloying for $Au_{0.8}Pd_{0.2}$-C catalysts, showing a low value of the extent of alloying ca. 0.14 (see Table 1).

Table 1: Crystallographic parameters for the Pd and $Au_{0.8}Pd_{0.2}$-C catalysts

Catalysts	2Theta (Degree)	d-spacing (Å)	Lattice parameter (Å)	Atomic radius (Å)	Intensity ratio [111] to [200]	Extent of alloying
Pd-C	45.76	1.981	3.962	1.401	2.732	
$Au_{0.8}Pd_{0.2}$-C	44.58	2.031	4.062	1.436	2.888	0.14
Pd (46-1043)	46.66	1.945	3.89	1.375		
Au (4-0784)	44.39	2.039	4.078	1.442		

The lattice contraction is due to the difference in lattice spacing between two metals in solution and is ascribed to Vegard's law [29]. The very low extent of alloying could be ascribed to the low-temperature synthesis route and suggests a bimetallic structure. The *d*-spacing value corresponding to the (200) plane is 2.031, which is a 0.39% deviation from the bulk Au reflection value. This indicates that the Pd nanoparticles in $Au_{0.8}Pd_{0.2}$-C catalyst were completely covered by the Au surface and shows exact crystal properties of the Au bulk (see Table 1).

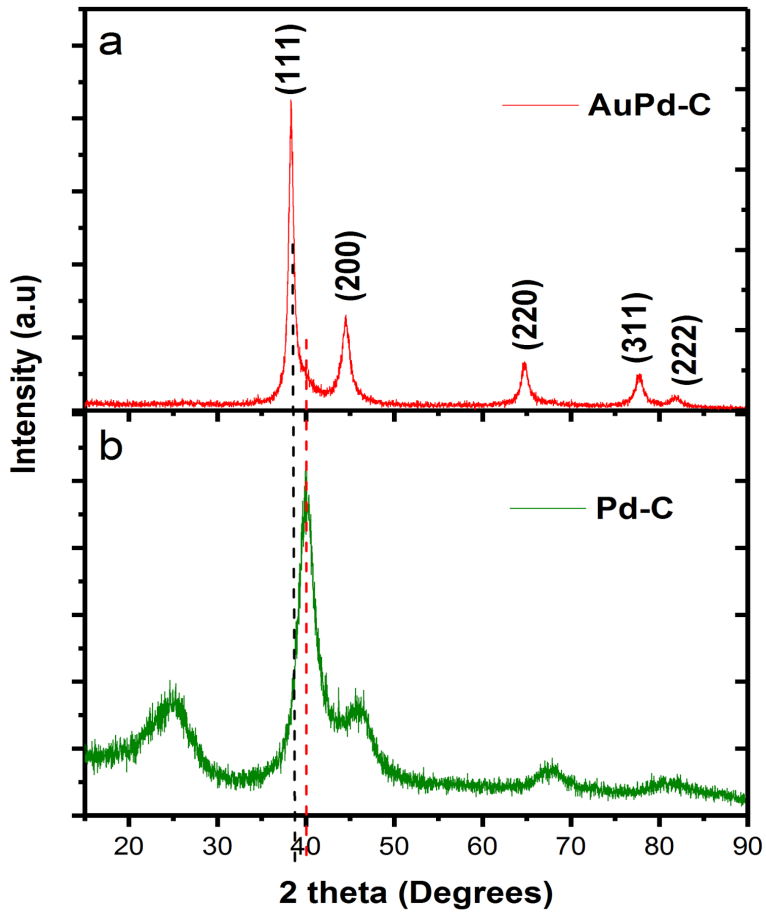

Figure. 2. The XRD patterns of $Au_{0.8}Pd_{0.2}$-C and Pd-C catalysts.

The marked decrease in the mean *d*-spacing could be attributed to the shift in the lattice contraction between the metals (Au, Pd) because of their difference in lattice spacing [29]. The data of the average crystallite sizes, lattice parameters, relative crystallinities and the interplanar distance (*d*-spacing) of the Pd and $Au_{0.8}Pd_{0.2}$-C catalysts are listed in Table 1.

3.2 Surface Morphology and Structure

The morphology and structure of the catalysts was studied using scanning electron microscopy (SEM), Energy dispersive X-ray spectroscopy (EDS), and Raman spectroscopy. As shown in Figure 3a, the SEM micrograph with corresponding EDS (Figure 3b) analysis of the $Au_{0.8}Pd_{0.2}$-C catalyst electrode is presented in Figure 3. The surface morphology of the $Au_{0.8}Pd_{0.2}$-C catalyst consists of spherical lumped nanoparticles with an average particle size of ca. 2.9 nm. The result of the EDS spectrum strongly verifies the co-existence of Au and Pd along with the presence of carbon black support. However, Pd traces are observed to be stronger than Au as illustrated in Figure 3 (b).

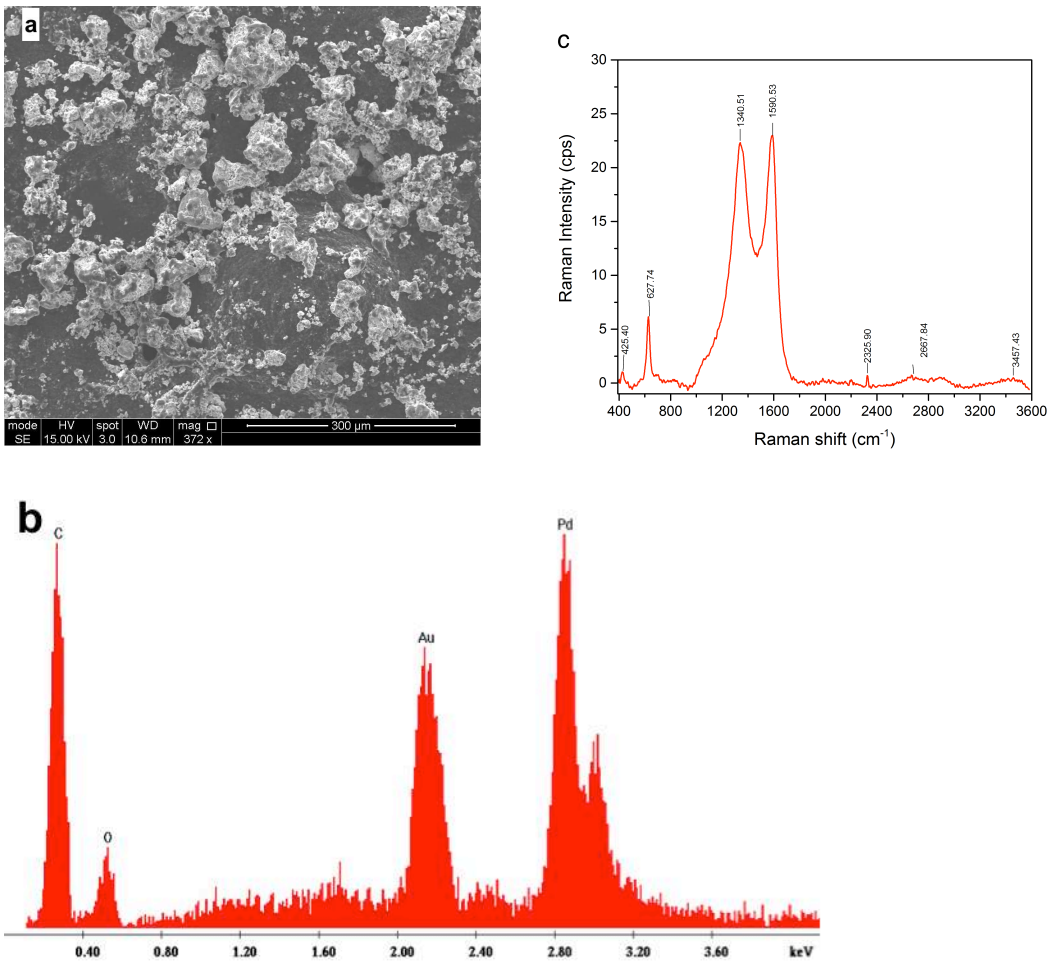

Figure 3: Images of the as-synthesised $Au_{0.8}Pd_{0.2}$-C: (a) SEM micrographs 300µm, (b) EDS trace indicating presence of $Au_{0.8}Pd_{0.2}$-C sample, (c) Raman spectroscopy.

For further chemical analysis, Raman spectroscopy was used. Raman spectroscopy is a powerful tool for identifying defective and disordered crystal structures. Figure 3c depicts the Raman spectrum collected between the ranges of 400 cm^{-1} - 3600 cm^{-1} for the $Au_{0.8}Pd_{0.2}$-C catalyst. The peaks at 1341 cm^{-1} and 1591 cm^{-1} are attributed to Au/C and Pd/C, respectively. The peaks between 400 to 800 cm^{-1} appeared due to CO stretching. The C-H and OH regions of stretching were also observed between 2000 – 2500 cm^{-1} and 3000 – 3600 cm^{-1}. Furthermore, it has been observed that there are more consistent peaks appearing at 1341 cm^{-1} and 1591 cm^{-1}, which may confirm the presence of both palladium (Pd) and gold (Au) ions in association with carbon (C) atoms [28, 30-35].

3.3 Electrocatalytic performance of $Au_{0.8}Pd_{0.2}$-C for formic acid oxidation

Figure 4 shows cyclic voltammograms and the catalytic activity of Pd-C and $Au_{0.8}Pd_{0.2}$-C catalysts in 1.0M KOH solution, at a scan rate of 20 mV s^{-1}. In the Pd-C catalyst, three potential peaks were observed (-0.79, -0.45, and 0.177 V), which were attributed to the reduction of Pd oxides generated during the positive scans [28]. The CV of Pd-C catalyst does not show the hydrogen adsorption/desorption peaks attributed to the formation of Pd oxides or adsorption of OH^- species on the Pd surface [36]. In the negative scan, there are three reduction peaks (-0.859, -0.556, and -0.283 V), which are attributed to the reduction of Pd oxides generated during the positive scan. In Pd-C catalysts, the shape and position of the reduction peaks depends on the reduction of nano-structured of the Pd (II) species (support from XRD, SEM). The electrochemically active surface area (ECSA) of the catalysts were estimated from the hydrogen adsorption/desorption peaks (coulombic charge) after subtraction of the double layer capacitance charge representing the number of active sites on the catalysts [20]. The evaluated ECSA's and other physicochemical properties of Pd-C and $Au_{0.8}Pd_{0.2}$-C are summarised in Table 2. It shows that $Au_{0.8}Pd_{0.2}$-C have larger ECSA compared to Pd-C, this is attributed to the synergetic property of the Au and Pd in the $Au_{0.8}Pd_{0.2}$-C electronic structure as Au loses valence electrons to Pd. This perturbation positively affects surface energy of Au to achieve improved electrochemical performance. Another reason for the higher electrochemically active surface area for $Au_{0.8}Pd_{0.2}$-C could be the enhanced metal surface site available for electrochemical reaction, which improve the catalytic properties [22]. The addition of a second metal creates active sites for the productions of reactive species (edges, corners, dendritic morphology) for enhance performance [37]. However, the chemical surface area (CSA) of the Pd-C (1.5 nm, 333.3 m^2g^{-1}) were higher than the $Au_{0.8}Pd_{0.2}$-C (2.9 nm, 172.4 m^2g^{-1}) catalysts due the the smaller particle size, which improve their electrochemical performance and stability in alkaline media.

Table 2: Physicochemical property of the catalysts

Catalysts	**Particle size, nm**	**ECSA, m^2g^{-1}**	**CSA, m^2g^{-1}**	**Metal surface site, gcat ($x10^{19}$)**
Pd-C	1.5	1.2	333.3	1.73
$Au_{0.8}Pd_{0.2}$-C	2.9	5.6	172.4	7.1

For the $Au_{0.8}Pd_{0.2}$-C catalysts, the peaks and shapes are dependent on the reduction of Au oxide. The main oxidation peaks for $Au_{0.8}Pd_{0.2}$-C catalyst are located at -0.841 and -0.059 V. At potentials above 0.3 V, this peak is associated with a process that has not been fully explained. It is widely accepted that OH^- is first chemisorbed in the initial stage of oxide formation and then transformed at higher potentials into a higher valence oxide [31, 36]. In the negative scan, there are two reduction peaks at -0.978 and -0.309 V, showing higher current density. The degree of enhancement towards KOH with the $Au_{0.8}Pd_{0.2}$-C catalyst was better than the Pd-C catalysts. The increase in the backward scan could be due to the modification of the electronic properties (bimetallic architecture) or the crystallographic orientation of $Au_{0.8}Pd_{0.2}$-C catalysts. A slight difference in the Pd-C voltammogram (Figure 4a) compared to $Au_{0.8}Pd_{0.2}$-C (Figure 4b) was observed. This is related to different Pd crystallite size; also, the addition of carbon can have an effect on the CV shape associated with hydrogen adsorption/desorption.

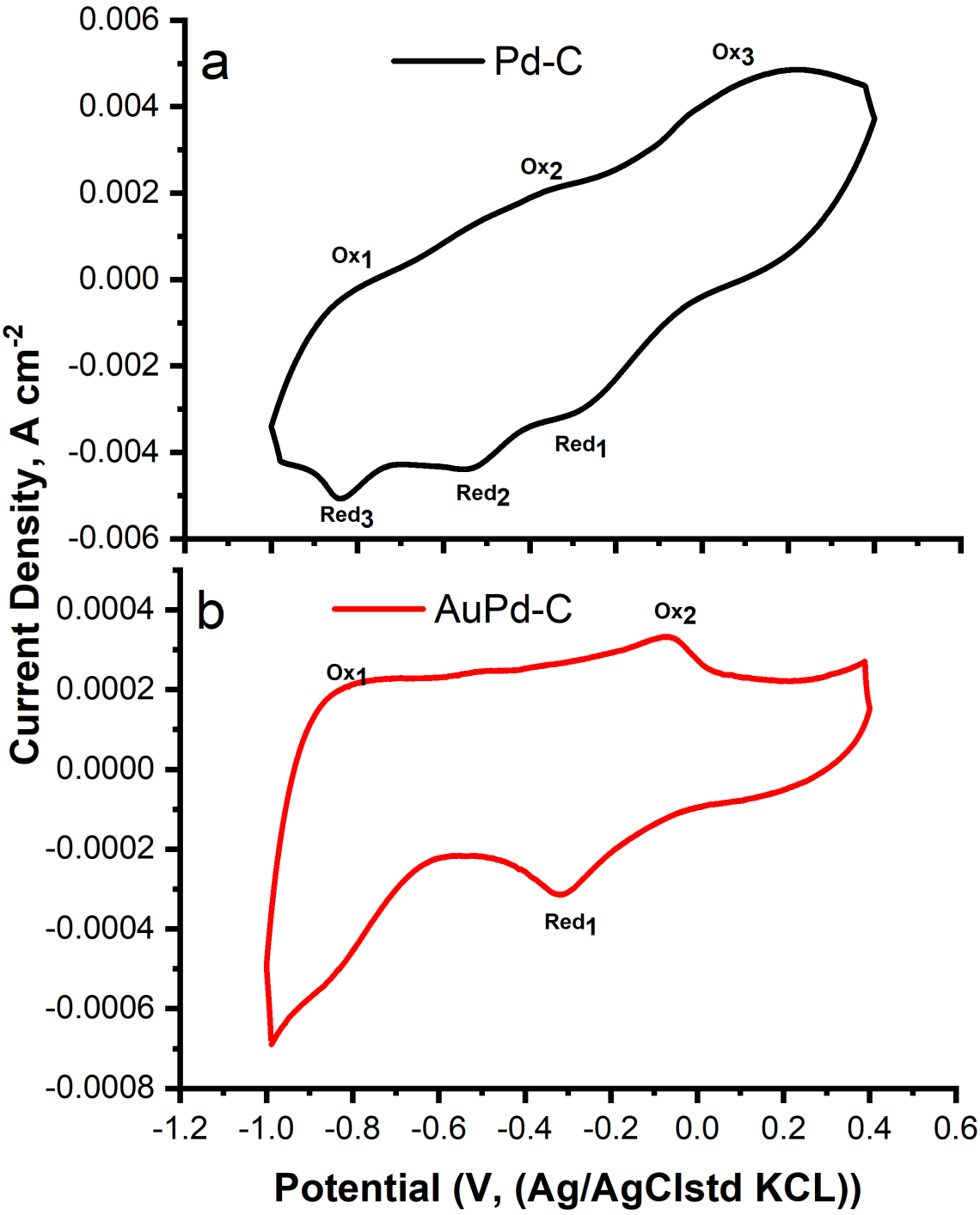

Figure 4: Cyclic voltammogram curves of Pd-C and $Au_{0.8}Pd_{0.2}$-C catalysts in 1.0M KOH solution at 25 ^{o}C, scan rate 20 mVs^{-1}.

This showed clearly that the synthesised bimetallic $Au_{0.8}Pd_{0.2}$-C catalyst shows higher attraction for hydroxyl group adsorption compared to the Pd-C catalyst. The presence of Au promotes a positive effect, which was confirmed by the appearance of a broad peak in the region of H_2 adsorption/desorption, suggesting that the H_2 adsorption/desorption processes on

the surface of catalyst were favored. The proposed enhanced properties are due to the electronic coupling between the bimetallic (Au and Pd), as well as the high catalytic activity of $Au_{0.8}Pd_{0.2}$-C catalysts. This performance depends on the lattice contraction associated with higher surface area and the formation of the Au and Pd bimetallic structure.

To investigate the stability of the catalysts, chronoamperometric analysis was performed at 0.3 V (vs. $Ag/AgCl_{sat.KCl}$ [0.197 V vs. NHE]). The stability experiments show that the Pd-C catalyst demonstrated superior catalytic stability in an alkaline medium compared to the $Au_{0.8}Pd_{0.2}$-C catalyst under similar conditions for all potentials (see Figure 5a). From Table 2, Pd-C catalysts show higher CSA (333 m3g-1) and particle size (1.5 nm) compared to $Au_{0.8}Pd_{0.2}$-C catalyst.

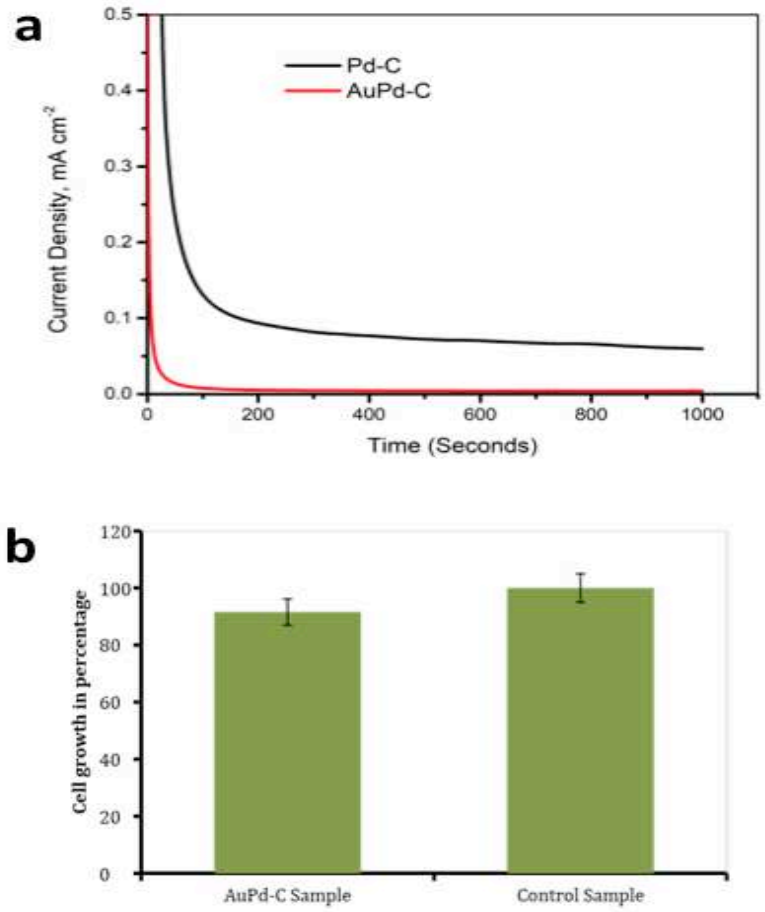

Figure 5: a) Chronoamperometric curve of the AuPd-C vs. Pd-C electrodes in a 1.0 M KOH solution at 0.3 V (vs. $Ag/AgCl_{sat.KCl}$ [0.197 V vs. NHE]) and room temperature. b) Biocompatibility analysis of AuPd-C sample with control group (without catalyst)

As can be seen, the Pd-C electrode displays a higher current density than the $Au_{0.8}Pd_{0.2}$-C electrode. This can be attributed to the smaller particle size and larger surface area of Pd-C (1.5 nm) compared to $Au_{0.8}Pd_{0.2}$-C (2.9 nm). The larger surface area of Pd-C confirms the very high electrochemical activity, which is consistent with the CV and XRD measurements.

3.4 Biocompatibility in physiological environment

Cell viability of the $Au_{0.8}Pd_{0.2}$-C sample was studied quantitatively with a standard MTT assay protocol. However, compared to the control group, a similar cellular response was observed (100% for the control group and 94% for the $Au_{0.8}Pd_{0.2}$-C specimen), as indicated in Figure 5b. In general, all results obtained are consistent with decreased solubility; therefore, it is thought that decreased ion release into cell medium occurred. This could create a favorable environment over the normal growth of cells. Moreover, orthopedically, the release of $Au_{0.8}Pd_{0.2}$-C ions with different concentrations encourages the process of osteo-integration, by depressing bone re-sorption, and also promotes further bone formation. Various researchers working on metal ions have proposed different formulations of gold and palladium in certain biomaterials, used in biomedical applications, which has demonstrated positive biocompatible behavior of both aforementioned metal ions. Liu *et al.,* proposed an immune-sensor based on N-(aminobutyl)-N-(ethylisoluminol) (ABEI), crowned with Au and Pd bimetallic nanoparticles, which exhibited a favorable biocompatibility. This immune-sensor was designed to root out human collagen type IV i.e. a biomarker related to diabetic nephropathy [34].

4 Conclusion

In the present study, $Au_{0.8}Pd_{0.2}$-C nanostructured catalyst has been investigated in order to determine its synergistic effects, bimetallic architecture and biocompatibility. Morphological examinations of the synthesized $Au_{0.8}Pd_{0.2}$-C catalyst, using SEM and XRD techniques, suggested that the produced catalyst is crystalline in nature, with spherical lumps of ca. 10.4 nm. Moreover, electrocatalytic performance analysis unveils that the $Au_{0.8}Pd_{0.2}$-C catalyst possesses greater attraction for OH groups increasing the positive potential, which could be due to the lattice contractions seen. However, Pd-C catalysts were found to be more chemically stable than $Au_{0.8}Pd_{0.2}$-C catalysts. The proposed nanostructured catalysts did not

affect the cellular growth when cultured for MTT assay, rendering it biocompatible to be used in medical applications. These findings can provide useful guidance for a simple design protocol for KOH oxidation and a promising tool for $Au_{0.8}Pd_{0.2}$-based materials for biocompatible applications. However, to reach the full potential of these catalysts in practical applications, a clear fundamental understanding on the effect of particle size on the electrochemical properties are required.

Acknowledgements

The authors gratefully acknowledge PhD funding support from Petroleum Technology Development Fund (PTDF) Scholarship of Nigeria and the University of Port Harcourt, Nigeria. Finally, the authors would like to thank Miss Alison R Thompson of the Department of Chemical & Biological Engineering, and Miss Xuzi Zhao, Syeda Mamoona Mateen of the Department of Material Sciences & Engineering, University of Sheffield, UK.

References

[1] Rees NV, Compton RG. Sustainable energy: a review of formic acid electrochemical fuel cells. Journal of Solid State Electrochemistry. 2011;15:2095-100.
[2] Mohammed YS, Mustafa MW, Bashir N. Hybrid renewable energy systems for off-grid electric power: Review of substantial issues. Renewable and Sustainable Energy Reviews. 2014;35:527-39.
[3] Yekini Suberu M, Wazir Mustafa M, Bashir N. Energy storage systems for renewable energy power sector integration and mitigation of intermittency. Renewable and Sustainable Energy Reviews. 2014;35:499-514.
[4] Posada JOG, Rennie AJR, Villar SP, Martins VL, Marinaccio J, Barnes A, et al. Aqueous batteries as grid scale energy storage solutions. Renewable and Sustainable Energy Reviews. 2017;68, Part 2:1174-82.
[5] Haruta M, Kobayashi T, Sano H, Yamada N. Novel Gold Catalysts for the Oxidation of Carbon Monoxide at a Temperature far Below 0 °C. Chemistry Letters. 1987;16:405-8.
[6] Haruta M. Size- and support-dependency in the catalysis of gold. Catalysis Today. 1997;36:153-66.
[7] Haruta M, Daté M. Advances in the catalysis of Au nanoparticles. Applied Catalysis A: General. 2001;222:427-37.
[8] Haruta M. Nanoparticulate Gold Catalysts for Low-Temperature CO Oxidation. Journal of New Materials for Electrochemical Systems. 2004;7:163-72.

[9] Hutchings GJ, Carrettin S, Landon P, Edwards JK, Enache D, Knight DW, et al. New approaches to designing selective oxidation catalysts: Au/C a versatile catalyst. Topics in Catalysis. 2006;38:223-30.
[10] Ivanova S, Bobadilla LF, Penkova A, Sarria FR, Centeno MA, Odriozola JA. Gold Functionalized Supported Ionic Liquids Catalyst for CO Oxidation. Catalysts. 2011;1:52-68.
[11] Posada JOG, Hall PJ. The Effect of Electrolyte Additives on the Performance of Iron Based Anodes for NiFe Cells. Journal of The Electrochemical Society. 2015;162:A2036-A43.
[12] Su D, McDonagh A, Qiao S-Z, Wang G. High-Capacity Aqueous Potassium-Ion Batteries for Large-Scale Energy Storage. Advanced Materials. 2017;29:1604007-n/a.
[13] Smith PM. The History and Use of Our Earth's Chemical Elements: A Reference Guide, 2nd Edition (Robert E. Krebs). Journal of Chemical Education. 2007;84:1767.
[14] Thakor AS, Jokerst J, Zavaleta C, Massoud TF, Gambhir SS. Gold Nanoparticles: A Revival in Precious Metal Administration to Patients. Nano Lett. 2011;11:4029-36.
[15] Siegel J, Kvítek Oe, Kolská Zk, Slepička P, Švorčík Vc. Gold Nanostructures Prepared on Solid Surface In: (Ed.) DYP, editor. Metallurgy - Advances in Materials and Processes2012.
[16] Fan JH, Hung WI, Li WT, Yeh JM. Biocompatibility Study of Gold Nanoparticles to Human Cells. In: Lim CT, Goh JCH, editors. 13th International Conference on Biomedical Engineering: ICBME 2008 3–6 December 2008 Singapore. Berlin, Heidelberg: Springer Berlin Heidelberg; 2009. p. 870-3.
[17] Murugan M, Anthony KJP, Jeyaraj M, Rathinam NK, Gurunathan S. Biofabrication of gold nanoparticles and its biocompatibility in human breast adenocarcinoma cells (MCF-7). Journal of Industrial and Engineering Chemistry. 2014;20:1713-9.
[18] Komarnicki P. Energy storage systems: power grid and energy market use cases. Archives of Electrical Engineering2016. p. 495.
[19] Orlando A, Colombo M, Prosperi D, Corsi F, Panariti A, Rivolta I, et al. Evaluation of gold nanoparticles biocompatibility: a multiparametric study on cultured endothelial cells and macrophages. Journal of Nanoparticle Research. 2016;18:58.
[20] Oseghale, Abdalla AH, Posada JOG, Hall PJ. A new synthesis route for sustainable gold copper utilization in direct formic acid fuel cells. International Journal of Hydrogen Energy. 2016;41:19394-6401.
[21] Shafique MA, Murtaza G, Saadat S, Uddin MKH, Ahmad R. Improved cell viability and hydroxyapatite growth on nitrogen ion-implanted surfaces. Radiation Effects and Defects in Solids. 2017:1-10.
[22] Chen S-S, Yang Z-Z, Wang A-J, Fang K-M, Feng J-J. Facile synthesis of bimetallic gold-palladium nanocrystals as effective and durable advanced catalysts for improved electrocatalytic performances of ethylene glycol and glycerol oxidation. Journal of Colloid and Interface Science. 2018;509:10-7.
[23] Liu M-T, Chen L-X, Li D-N, Wang A-J, Zhang Q-L, Feng J-J. One-pot controlled synthesis of AuPd@Pd core-shell nanocrystals with enhanced electrocatalytic performances for formic acid oxidation and glycerol oxidation. Journal of Colloid and Interface Science. 2017;508:551-8.
[24] Xu JB, Zhao TS, Liang ZX. Carbon supported platinum–gold alloy catalyst for direct formic acid fuel cells. Journal of Power Sources. 2008;185:857-61.
[25] Yang Z-Z, Liu L, Wang A-J, Yuan J, Feng J-J, Xu Q-Q. Simple wet-chemical strategy for large-scaled synthesis of snowflake-like PdAu alloy nanostructures as effective

electrocatalysts of ethanol and ethylene glycol oxidation. International Journal of Hydrogen Energy. 2017;42:2034-44.
[26] Al-Akraa IM, Mohammad AM, El-Deab MS, El-Anadouli BE. Electrocatalysis by design: Synergistic catalytic enhancement of formic acid electro-oxidation at core–shell Pd/Pt nanocatalysts. International Journal of Hydrogen Energy. 2015;40:1789-94.
[27] Liu, Wang L, Wang G, Deng C, Wu B, Gao Y. High active carbon supported PdAu catalyst for formic acid electrooxidation and study of the kinetics. Journal of Physical Chemistry C. 2010;114:21417-22.
[28] Lin X-X, Zhang X-F, Wang A-J, Fang K-M, Yuan J, Feng J-J. Simple one-pot aqueous synthesis of AuPd alloy nanocrystals/reduced graphene oxide as highly efficient and stable electrocatalyst for oxygen reduction and hydrogen evolution reactions. Journal of Colloid and Interface Science. 2017;499:128-37.
[29] Ren M, Zhou Y, Tao F, Zou Z, Akins DL, Yang H. Controllable Modification of the Electronic Structure of Carbon-Supported Core–Shell Cu@Pd Catalysts for Formic Acid Oxidation. The Journal of Physical Chemistry C. 2014;118:12669-75.
[30] Dong J, Ozaki Y, Nakashima K. Infrared, Raman, and Near-Infrared Spectroscopic Evidence for the Coexistence of Various Hydrogen-Bond Forms in Poly(acrylic acid). Macromolecules. 1997;30:1111-7.
[31] Saha D, Deng S. Hydrogen Adsorption on Ordered Mesoporous Carbons Doped with Pd, Pt, Ni, and Ru. Langmuir. 2009;25:12550-60.
[32] Zhang P, Shao C, Zhang Z, Zhang M, Mu J, Guo Z, et al. In situ assembly of well-dispersed Ag nanoparticles (AgNPs) on electrospun carbon nanofibers (CNFs) for catalytic reduction of 4-nitrophenol. Nanoscale. 2011;3:3357-63.
[33] Chi Y, Zhao L, Yuan Q, Yan X, Li Y, Li N, et al. In situ auto-reduction of silver nanoparticles in mesoporous carbon with multifunctionalized surfaces. Journal of Materials Chemistry. 2012;22:13571-7.
[34] Li J-G, Tsai C-Y, Kuo S-W. Fabrication and Characterization of Inorganic Silver and Palladium Nanostructures within Hexagonal Cylindrical Channels of Mesoporous Carbon. Polymers. 2014;6:1794.
[35] Kiefer J. Recent Advances in the Characterization of Gaseous and Liquid Fuels by Vibrational Spectroscopy. Energies. 2015;8:3165.
[36] Cerritos RC, Guerra-Balcázar M, Ramírez RF, Ledesma-García J, Arriaga LG. Morphological Effect of Pd Catalyst on Ethanol Electro-Oxidation Reaction. Materials. 2012;5:1686-97.
[37] Friend CM, Hashmi ASK. Gold Catalysis. Accounts of Chemical Research. 2014;47:729-30.